

Chapter 5

Migration in MgAl_2O_4 Spinel

5.1 Introduction

Defect formation energy calculations such as those described in section 2.7 can be used to evaluate saddle point energies for migration pathways. For transport occurring via a thermally activated hopping process, the migration activation energy is defined as the difference between the energy of the migrating species at the saddle point and its minimum energy fully relaxed within the lattice. This migration energy is related to the activation energy for transport as described in the introduction.

The height of the barrier is established by running a number of defect calculations in which the position of the migration species is fixed while the surrounding lattice is relaxed. The process of finding the migration barrier is

as follows: an initial trial path is defined, usually a straight line between the start and end positions and the energy of the defect is evaluated at a number of positions along this path. The position giving rise to the maximum value of the energy along this path is then an initial estimate for the saddle point. A grid of positions in the plane perpendicular to the initial trial path, at this initial maximum is defined and energies calculated to form the defect state associated with the migrating species in these positions. Subsequently a contour plot of energies is calculated, ideally this will be in the form of a sinkhole with the minimum at the initial estimated location, in which the barrier height has been found; otherwise a new estimate is established and a calculations on a second trial path are made. Provided that this second estimate of the saddle point is the maximum of the new trial path, the real saddle point and the barrier height have been found. If a new maximum is found then a new perpendicular plane must be evaluated and this process continues in an iterative fashion until the saddle point is established to the desired degree of accuracy.

In some cases energies in a plane parallel to the migration pathway have also been evaluated, while not strictly necessary to calculate the energy barrier they do provide some insight as to the shape of the energy landscape.

Clearly this scheme has the potential to be very time consuming, involving many different calculations to establish a single barrier. Fortunately for most of the pathways calculated here the degree of symmetry is such that either the initial trial saddle point is correct, or the true saddle point lies in the

same plane as the initial trial point. In addition to its computationally wasteful nature, a further fault with this scheme is that it assumes both the start and end points for migrations. While this is unlikely to cause problems when considering simple isolated vacancy and interstitial mechanisms, as calculated here, it could not identify more complex modes involving multiple simultaneous hops, such as those reported by Uberuaga *et al.* [140] for MgO which were calculated using temperature accelerated dynamics [141, 142].

Migration energies have been evaluated for all vacancy and interstitial defects defined in chapter 4. Due to the prevalence of antisite defects a number of mechanisms involving antisite defects have been considered. For example, a Mg^{2+} hopping from the magnesium sublattice to a V''_{Al} and an Al^{3+} hopping from the aluminium sublattice to a V''_{Mg} . Both the above defects create new antisite defects (or in reverse destroy existing ones), they also allow vacancies to switch between the two cation sublattices. Another pair of possibilities are that of an Al_{Mg} antisite moving to a V''_{Mg} or a Mg'_{Al} hopping to a V'''_{Al} . These two mechanisms are analogous to ordinary vacancy migration but are mediated by an antisite defect. Throughout this chapter energies are given with respect to the starting stable configuration, i.e. the energy quoted at a migration saddle point is the difference between the energy required for the defect to form at the saddle point minus the energy required to form the initial configuration. In contrast to previous chapters, none of the calculations presented here involved a shell model.

5.2 Vacancy Migration

5.2.1 Magnesium Vacancy

Magnesium ions in MgAl_2O_4 spinel occupy equivalent sites as listed in table 3.1. The arrangement of ions is such that from a given lattice site the nearest neighbour sites are equivalent i.e. there is only one possible migration mechanism. Taking the Mg^{2+} ion at $(0, 0, 0)$ as a start point with a vacancy at $(\frac{1}{4}, \frac{1}{4}, \frac{1}{4})$ the Mg^{2+} ion hops into the vacant site in the $[111]$ direction, or equivalently the vacancy hops from $(\frac{1}{4}, \frac{1}{4}, \frac{1}{4})$ to $(0, 0, 0)$. A local minimum is found at $(\frac{1}{8}, \frac{1}{8}, \frac{1}{8})$ therefore two equivalent saddle points exist. The analysis described above finds these to be at $(0.08, 0.08, 0.08)$ and $(0.16, 0.16, 0.16)$. The contour plot in figure 5.1 shows that the energy profile perpendicular to the ion's migration pathway while figure 5.2 is the profile in the migration plane. The saddle points (marked by crosses in figure 5.2 are 0.65eV higher in energy than the minima and there is a local minimum (the central filled square in figure 5.2) at a height of 0.55eV. The energy profile along the predicted migration pathway is as shown in figure 5.3.

As noted previously it is also possible for a V''_{Mg} to migrate by exchanging sites with an Al_{Mg} antisite defect. This hop is analogous to the normal V''_{Mg} migration discussed above and the energy profiles perpendicular to, (see figure 5.4) and in the plane of, migration (see figure 5.5) are qualitatively very similar to the previous case. The saddle points are located at $(0.07, 0.07, 0.07)$ and $(0.16, 0.16, 0.16)$ with a height of 1.15eV. As in the normal

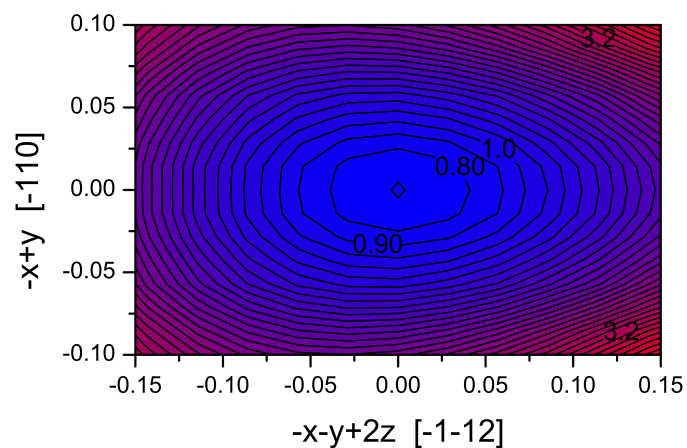


Figure 5.1: Energy contour plot for Mg^{2+} migration via a magnesium vacancy mechanism, perpendicular to the migration pathway.

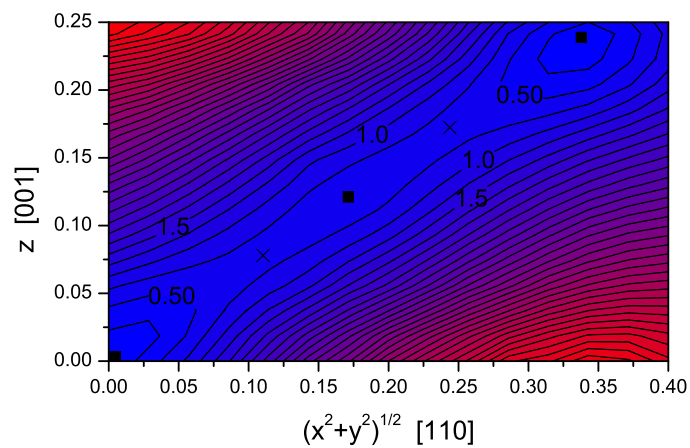


Figure 5.2: Energy contour plot for Mg^{2+} migration via a magnesium vacancy mechanism, parallel to the migration pathway.

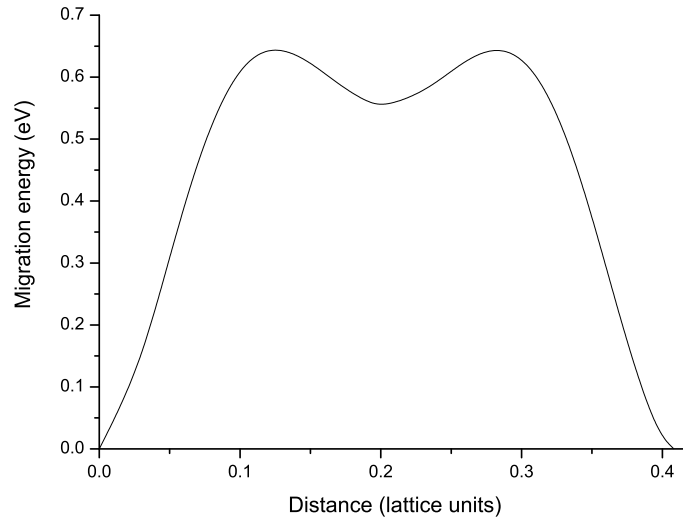


Figure 5.3: Migration energy for Mg^{2+} ion moving on Mg sublattice via vacancy mechanism

V''_{Mg} mechanism there is a saddle point located when the migrating Al^i_{Mg} is halfway between its start and end points. Figure 5.6 shows that this well is proportionately much deeper than for the normal V''_{Mg} migration, being only 0.67eV higher in energy than the starting configuration.

5.2.2 Aluminium Vacancy

Aluminium ions in MgAl_2O_4 spinel occupy equivalent sites as listed in table 3.1. As for magnesium the arrangement of ions is such that all of the aluminium sites which are nearest neighbour to a given V'''_{Al} are equivalent with respect to that vacant site. An example configuration is for a Al^{3+} at $(\frac{3}{8}, \frac{3}{8}, \frac{5}{8})$ to hop along [110] to a V'''_{Al} at $(\frac{5}{8}, \frac{5}{8}, \frac{5}{8})$. The energy profile (figure 5.7) perpendicular to the migration pathway shows that this migration mechanism

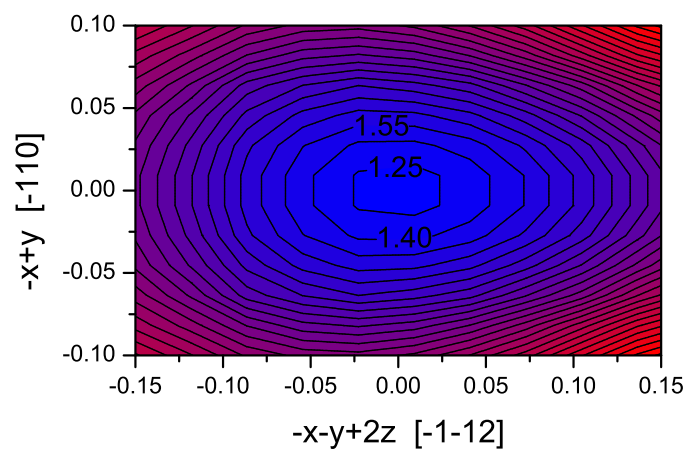


Figure 5.4: Energy contour plot for Al^{3+} migration via a magnesium vacancy mechanism, perpendicular to the migration pathway.

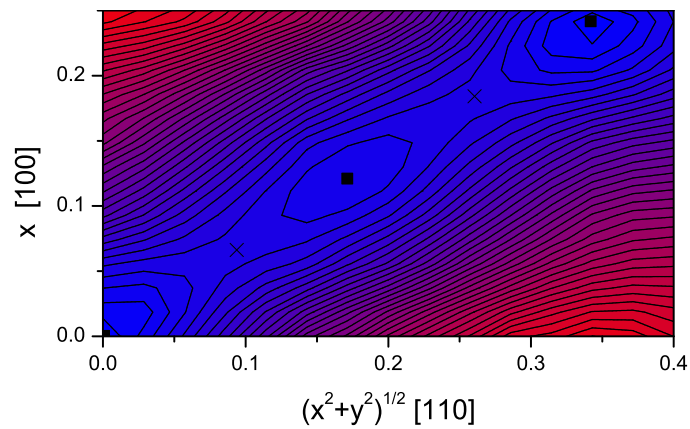


Figure 5.5: Energy contour plot for Al^{3+} migration via a magnesium vacancy mechanism, parallel to the migration pathway.

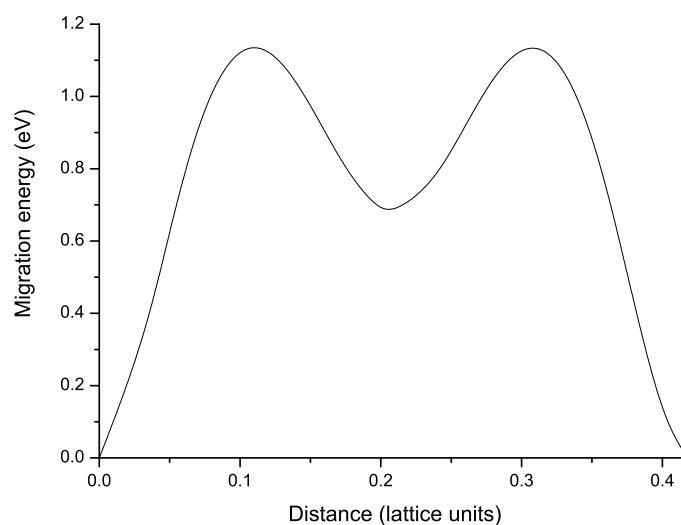


Figure 5.6: Migration energy for Al^{3+} ion moving on Mg sublattice via vacancy mechanism.

deviates from a straight line, in the $[001]$ direction. Figure 5.8 places the region covered by figure 5.7 in the context of the perfect lattice positions of atoms in the (110) plane. Considering again figure 5.7, it is evident that, due to the perfect lattice relaxation of surrounding oxygen ions, the $[001]$ deviation in the migration pathway means that the migrating ion does not pass so closely to lattice ions.

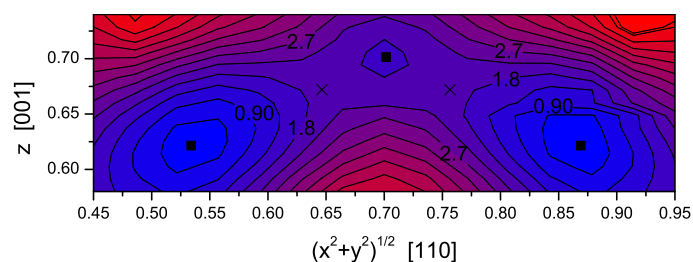


Figure 5.7: Energy contour plot for Al^{3+} migration via an aluminium vacancy mechanism, parallel to the migration pathway.

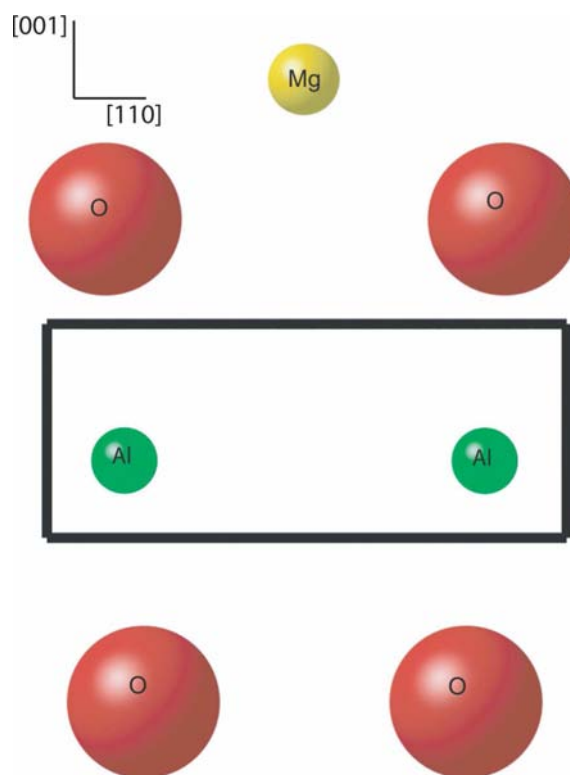


Figure 5.8: Ion positions local to aluminium vacancy migration. The region surveyed in figure 5.7 is marked by a black outline.

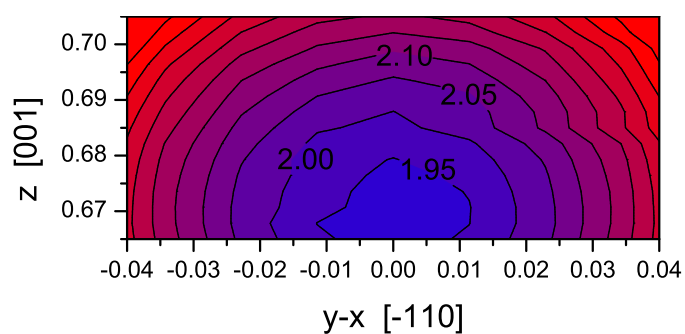


Figure 5.9: Energy contour plot for Al^{3+} migration via an aluminium vacancy mechanism, perpendicular to the migration pathway.

The energy profile perpendicular to the migration pathway at the saddle points is illustrated by figure 5.9. Figure 5.10 shows the energy profile along the predicted migration pathway. As with the V''_{Mg} mechanisms the path is symmetrical with two saddle points surrounding a central local minimum. The saddle points are located at (0.46, 0.46, 0.67) and (0.54, 0.54, 0.54) and require an activation energy of 1.94eV to cross. This is considerably higher than the activation energies for migration on the magnesium sublattice. Comparing this barrier to the one determined in figure 5.6 for the migration of aluminium on the magnesium sublattice, the difference is 0.79 eV (i.e. 1.94 eV - 1.15 eV). In contrast, the normalised formation energy of a Al_{Mg} defect, formed as part of the antisite reaction, equation 4.1, is 0.77 eV (table 4.2) combining these it is clear that the transport of Al^{3+} will occur not on its native sublattice but instead on the magnesium sublattice.

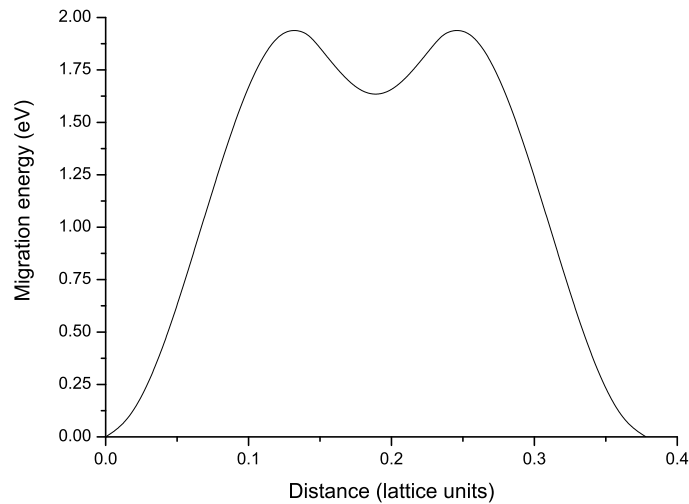


Figure 5.10: Migration energy for Al^{3+} ion moving on Al sublattice via vacancy mechanism

As with magnesium migration, it is possible to define an alternative mechanism involving an antisite defect; in this case a Mg'_{Al} replaces the migrating Al^{3+} ion. The energy contours perpendicular (see figure 5.11) and parallel (see figure 5.12) to the migration pathway shows a similar profile to the normal V'''_{Al} migration. The saddle points were found at $(0.46, 0.46, 0.69)$ and $(0.54, 0.54, 0.69)$, and the predicted barrier is 0.85 eV. The central local minimum is shallower than for the normal aluminium vacancy case. The energy profile along the migration path is displayed in figure 5.13. Similarly to migration on the magnesium sublattice, this barrier to migration for a Mg^{2+} is considerably less than for the more highly charged Al^{3+} . Nevertheless it is clear that Mg^{2+} migration will occur predominantly via the magnesium sublattice.

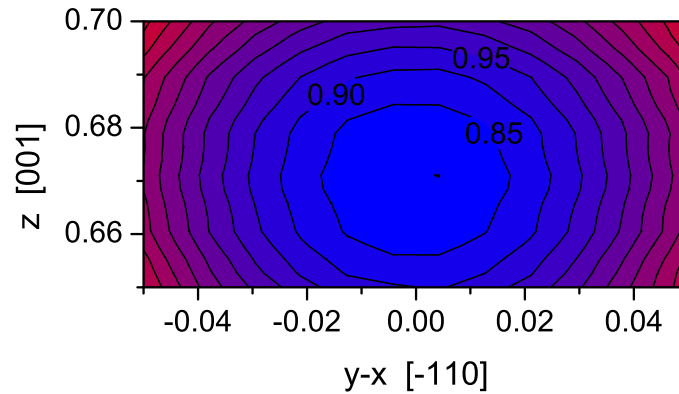


Figure 5.11: Energy contour plot for Mg^{2+} migration via an aluminium vacancy mechanism, perpendicular to the migration pathway.

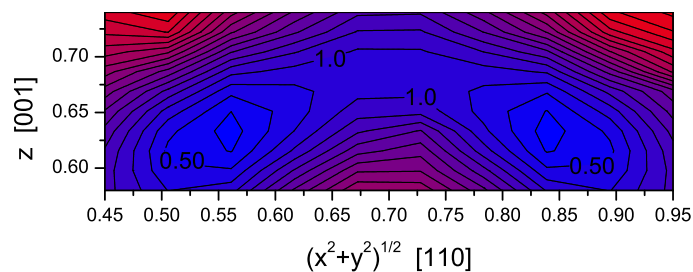


Figure 5.12: Energy contour plot for Mg^{2+} migration via an aluminium vacancy mechanism, parallel to the migration pathway.

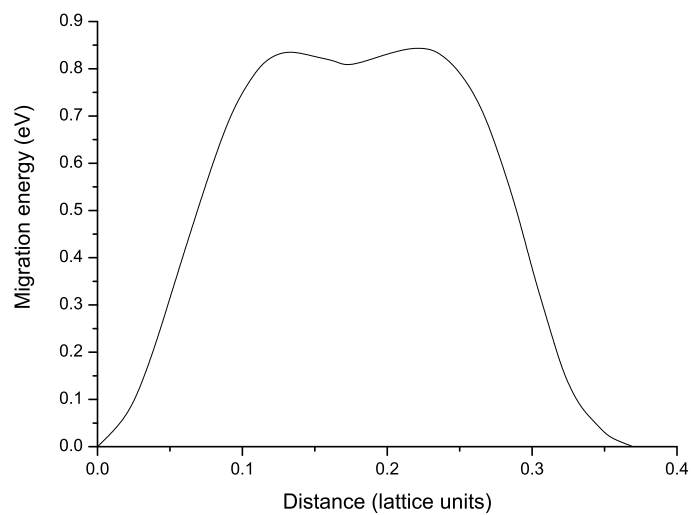


Figure 5.13: Migration energy for Mg^{2+} ion moving on Al sublattice via vacancy mechanism

5.2.3 Inter-Cation Sublattice Vacancy Mechanisms

The mechanisms considered thus far all conserve the type and number of defects involved, however, because MgAl_2O_4 has two distinct cation sublattices and a low antisite energy it is expected that a vacancy might transfer from one to the other. There are two possibilities,



and,



These mechanisms are important because they create (and in reverse, destroy) antisite defects. As can be seen from figure 5.8, a straight line between the two defects brings the migrating ion very close to an oxygen lattice site, consequently substantial deviation from this line is expected.

Al_{Mg}' Creation Via V_{Mg}'' Transport

For this mechanism, as described in equation 5.1, the migrating species is an Al^{3+} which is initially on the aluminium sublattice but finishes on the magnesium sublattice. Assuming that the migration path takes place in the plane shown in figure 5.8, with the migrating Al^{3+} ion initially at $(\frac{5}{8}, \frac{5}{8}, \frac{5}{8})$ movement to a vacant magnesium site at $(\frac{1}{2}, \frac{1}{2}, 1)$ generates the contour map figure 5.14. There are two maxima, though one is higher than the other, with (obviously) a local minimum between them.

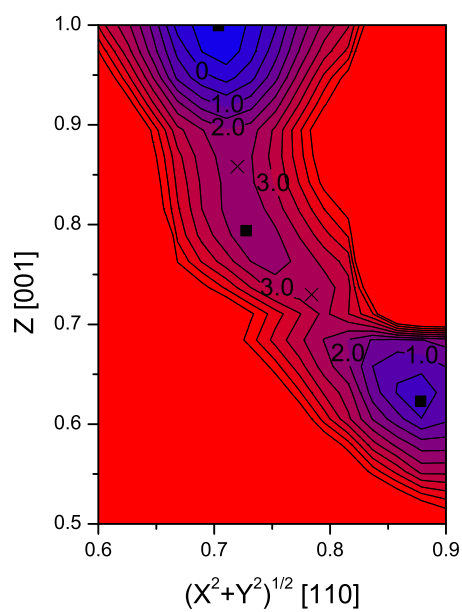


Figure 5.14: Energy contour plot parallel to a hop via the mechanism described by equation 5.1. The initial conditions place the migrating Al^{3+} on its native lattice site, i.e. in the bottom right corner.

The two oppositely charged defects which are formed, are a bound pair and are lower in energy than the initial vacancy as can be inferred from tables 4.1 and 4.5. The energy in the plane perpendicular to the migration, at the higher saddle point, is shown in figure 5.15. Since this plot shows a minimum when $x=y$ it confirms that the pathway at this saddle point is in the plane of figure 5.14, however, the plot perpendicular to the migration path at the lower minimum (figure 5.16) shows two distinct minima so the migrating ion deviates from the assumed plane after passing the local minimum.

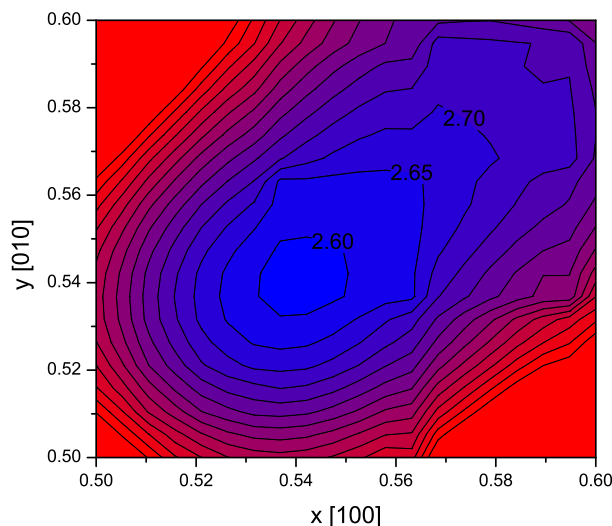


Figure 5.15: Energy contour plot perpendicular to a hop via the mechanism described by equation 5.1, higher saddle point.

The higher maximum is at $(0.55, 0.55, 0.72)$ and is 2.66 eV higher in energy than the initial conditions, the lower at $(0.52, 0.49, 0.84)$ with a barrier of 2.24 eV and the local minimum at $(0.51, 0.51, 0.79)$, 2.04 eV higher in energy than the initial conditions. The energy profile along the pathway is displayed in figure 5.17. These energies are higher than those associated with migration

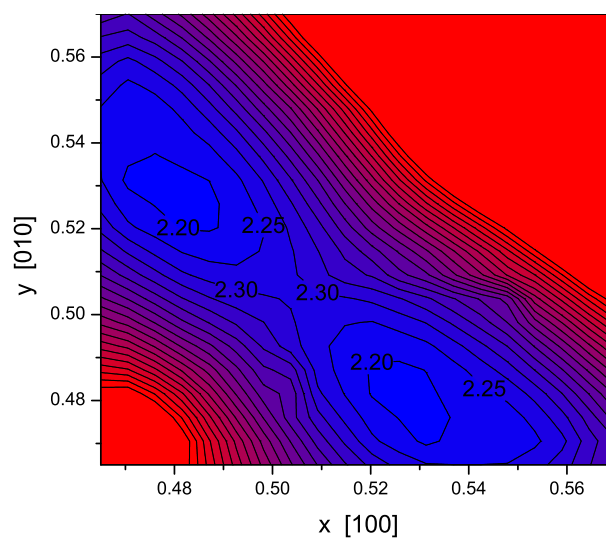


Figure 5.16: Energy contour plot perpendicular to a hop via the mechanism described by equation 5.1, lower saddle point.

purely on the magnesium or aluminium sublattices.

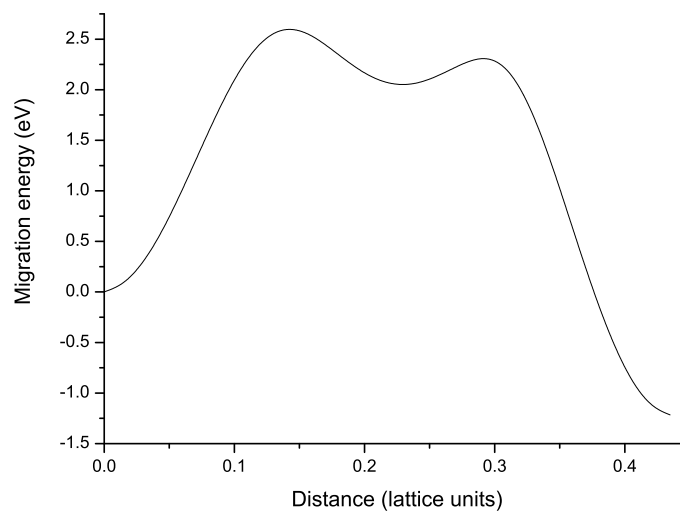


Figure 5.17: Migration energy for Al^{3+} ion moving between Al and Mg sublattices via vacancy mechanism.

Mg'_{Al} Creation Via V'''_{Al} Transport

This mechanism corresponds to equation 5.2; the migrating species is an Mg^{2+} ion which is initially on the magnesium sublattice then moves into a vacancy on the aluminium sublattice. Taking the magnesium site to be $(\frac{1}{2}, \frac{1}{2}, 1)$ and the V'''_{Al} to be at $(\frac{5}{8}, \frac{5}{8}, \frac{5}{8})$ the energy profile in the plane of migration is shown in figure 5.18, the path is similar to that in section 5.2.3 but there is only one saddle point, at $(0.56, 0.56, 0.73)$ providing a high barrier of 3.32 eV. The energy profile in the plane perpendicular to the pathway at this saddle point is contained in figure 5.19 The final configuration is higher in energy than the initial one by 2.17 eV, this leads to a significant asymmetry in the energy profile, see figure 5.20.

5.2.4 Oxygen Vacancy

As discussed in section 3.1.1 the oxygen ions in spinel relax from their idealised positions according to the u parameter. The effect of these relaxations is shown in figure 5.21. From a given oxygen site there are three different possible hops, numbered 1 to 3, where each migration corresponds to the O^{2-} ion at the centre moving onto a vacant site, which in the case of mechanism 1 would be the site indicated by the arrow labeled 1. It is important to notice that while mechanism 1 will allow the migrating vacancy to traverse the lattice neither mechanism 2 or 3 alone provides a continuous pathway although they can form part of a contiguous pathway in concert with mechanism 1 or

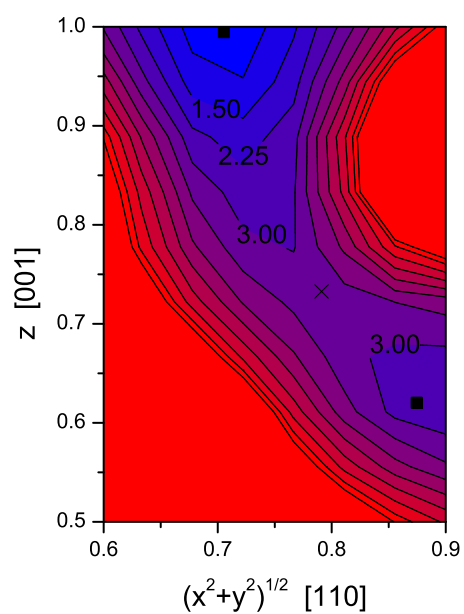


Figure 5.18: Energy contour plot parallel to a hop via the mechanism described by equation 5.2. The initial conditions place the migrating Mg^{2+} on its native lattice site, i.e. in the top centre.

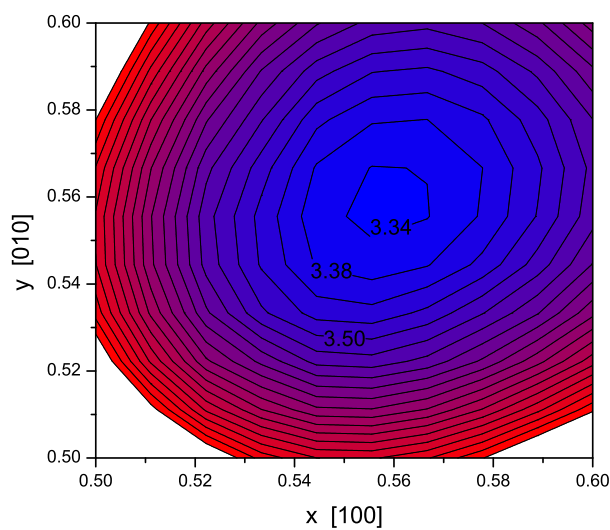


Figure 5.19: Energy contour plot parallel to a hop via the mechanism described by equation 5.2. The initial conditions place the migrating Mg^{2+} on its native lattice site, i.e. in the top centre.

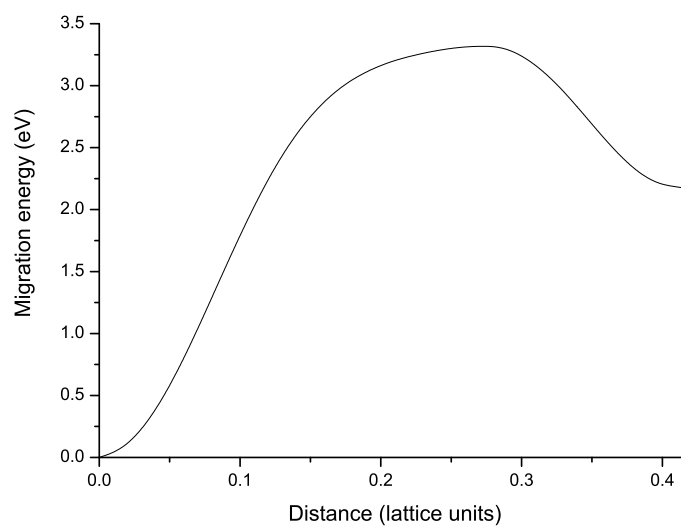


Figure 5.20: Migration energy for Mg^{2+} ion moving between Mg and Al sublattices via vacancy mechanism.

each other.

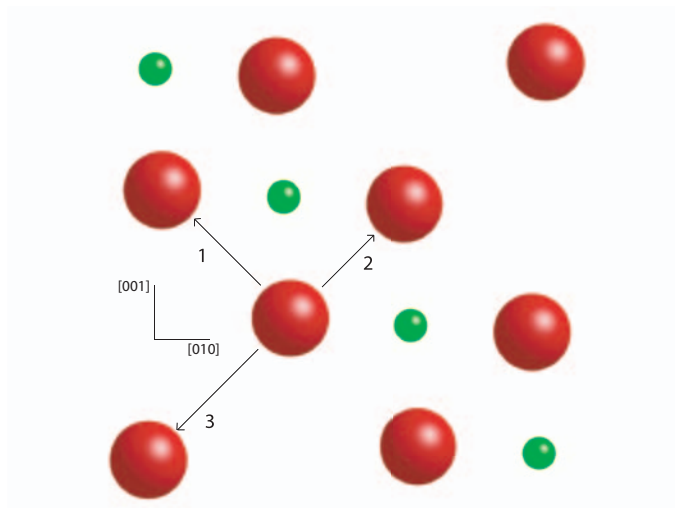


Figure 5.21: Cross section through a single unit cell of spinel in the $[100]$ plane. The labeled arrows show the three different possible hops from a chosen oxygen site.

Mechanism 1

This migration pathway is in a plane (figure 5.22) like that in figure 5.21 but rotated through 90° . The distortion from a straight line occurs because the migrating ion deviates to avoid moving very close to the neighbouring Al^{3+} .

Unlike with the majority of the cation vacancy migration mechanisms there is no local minimum, instead there is a single saddle point at the point marked by the cross in figure 5.22; the barrier height is 1.68 eV. The location of this saddle point is confirmed by figure 5.23. This figure is higher than that for both cations migrating on the magnesium sublattice, though is lower than

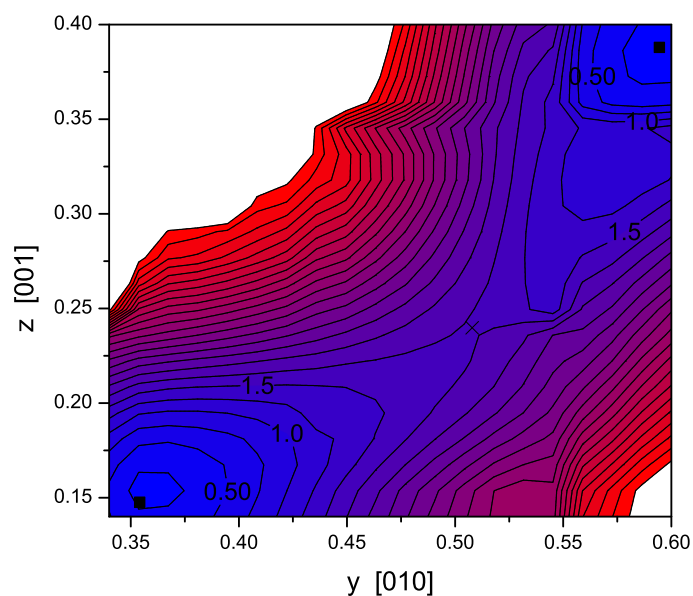


Figure 5.22: Energy contour plot for O^{2-} migration via oxygen vacancy mechanism 1, parallel to the migration pathway.

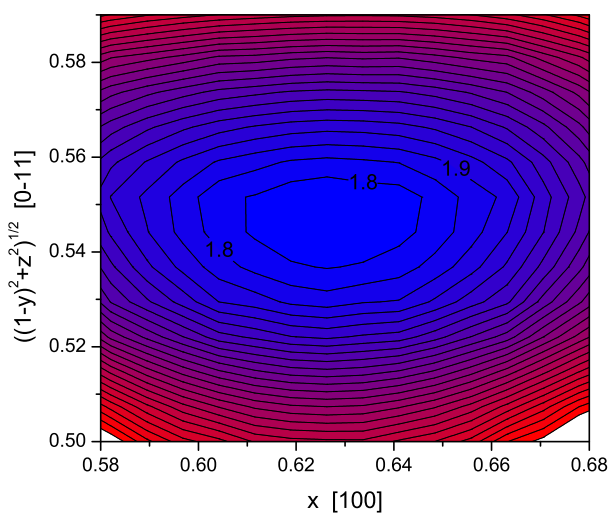


Figure 5.23: Energy contour plot for O^{2-} migration via oxygen vacancy mechanism 1, perpendicular to the migration pathway.

for Al^{3+} migrating on its native sublattice. Figure 5.24 shows that the path is symmetric with the saddle point halfway along its length.

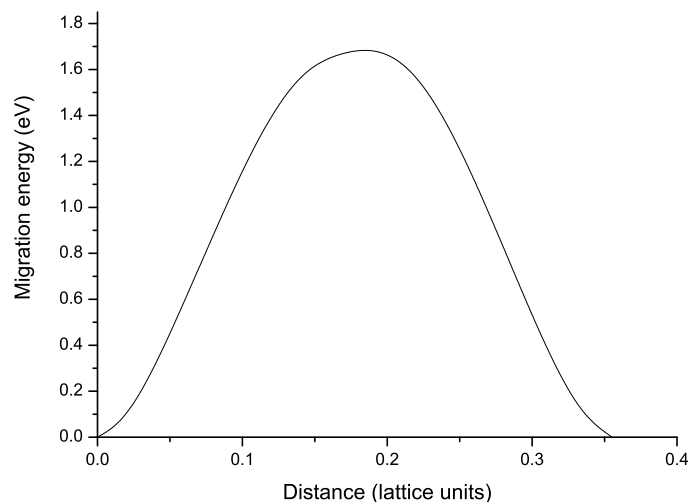


Figure 5.24: Migration energy for O^{2-} ion moving on O sublattice via vacancy mechanism 1.

Mechanism 2

Mechanism 2 is the shortest of the three hops as the two ions involved are pulled together due to their sharing of the same pair of aluminium ions as nearest neighbours. This pathway is in the plane perpendicular to that illustrated by figure 5.21, alternatively, the two sites involved are the bottom two oxygen sites in figure 5.8.

Figure 5.25 shows that the path is very nearly straight. There is only one saddle point, halfway along the symmetric path (figure 5.26). Figure 5.27 confirms that this saddle point lies in the plane of figure 5.25. The activation energy for this mechanism is 1.53 eV.

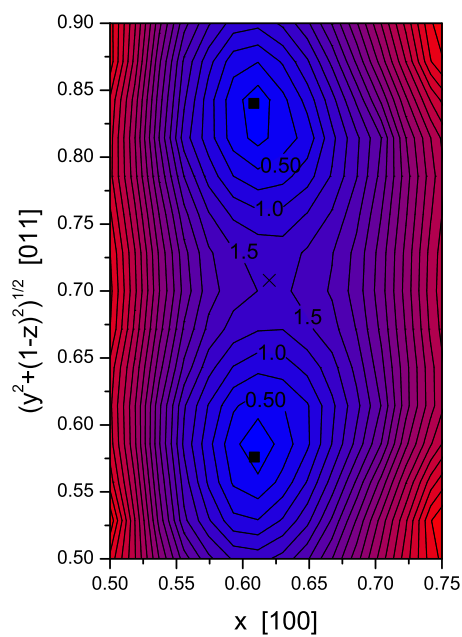


Figure 5.25: Energy contour plot for O^{2-} migration via oxygen vacancy mechanism 2, parallel to the migration pathway.

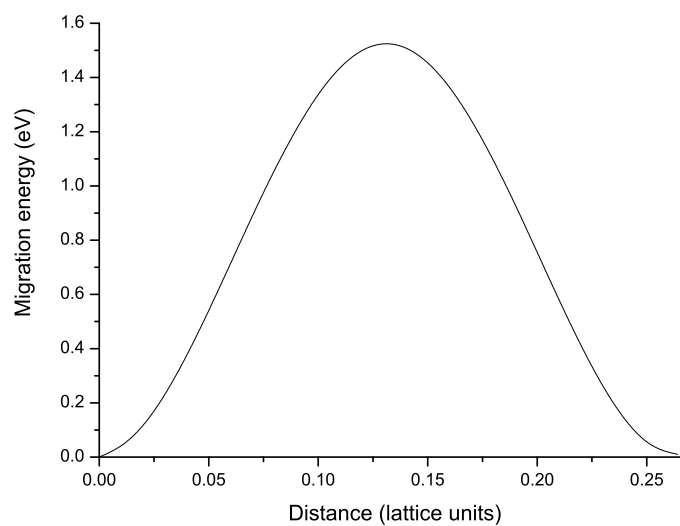


Figure 5.26: Migration energy for O^{2-} ion moving on O sublattice via vacancy mechanism 2.

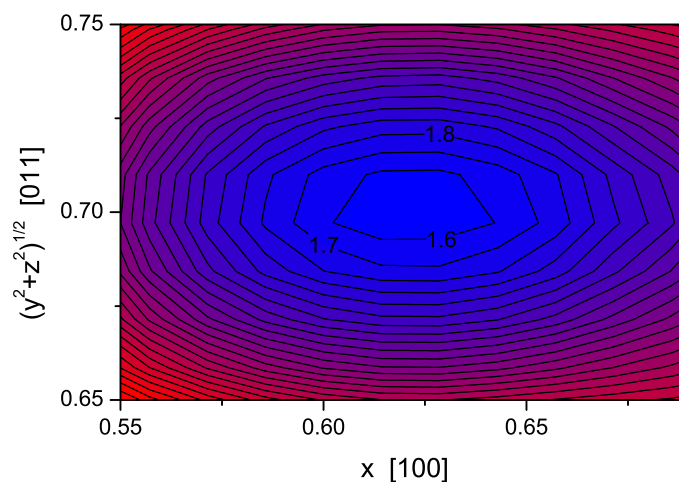


Figure 5.27: Energy contour plot for O^{2-} migration via oxygen vacancy mechanism 2, perpendicular to the migration pathway.

Mechanism 3

Lattice relaxation makes the pathway taken by the migrating ion in mechanism 3 the longest of the three oxygen vacancy pathways. The two sites are the upper pair of oxygen ions in figure 5.8, the deviation from straight shown in figure 5.28 and the asymmetry in figure 5.29 is a consequence of the proximity of the magnesium site. Figure 5.30 shows that the pathway is again symmetric with a single saddle point. The activation energy is substantially higher than for the other two mechanisms, 3.64 eV.

Comparing the three mechanisms, though mechanism 2 has the smallest activation energy it does not provide a continuous pathway through the lattice, thus it is mechanism 1 which is responsible for determining the activation energy of oxygen vacancy transport in this material.

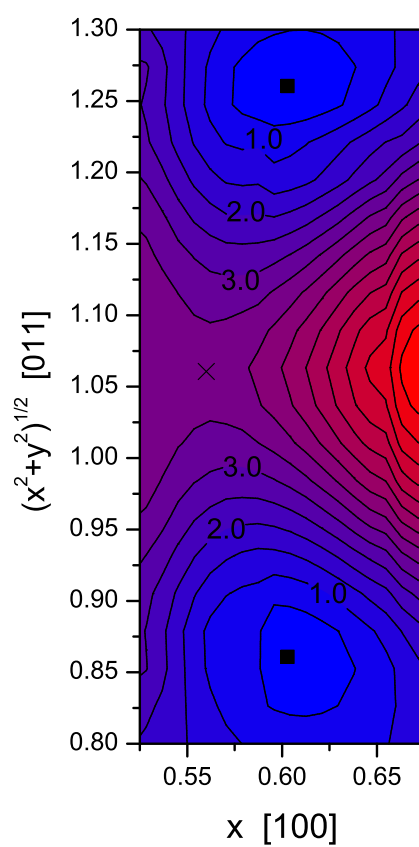


Figure 5.28: Energy contour plot for O^{2-} migration via oxygen vacancy mechanism 3, parallel to the migration pathway.

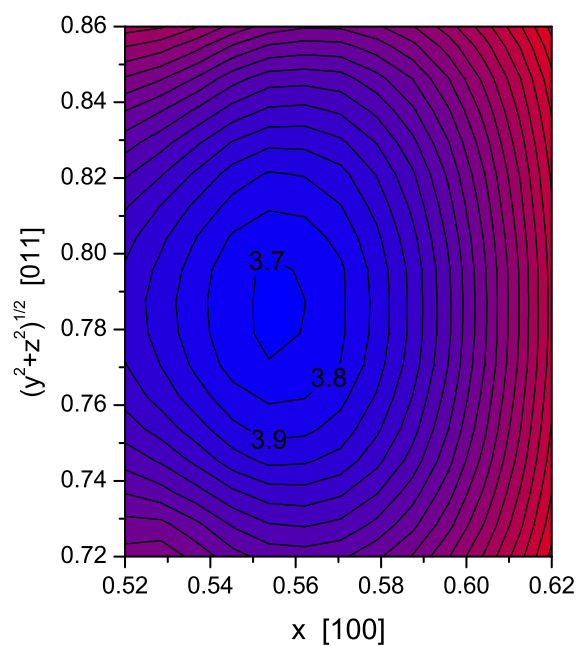


Figure 5.29: Energy contour plot for O^{2-} migration via oxygen vacancy mechanism 3, perpendicular to the migration pathway.

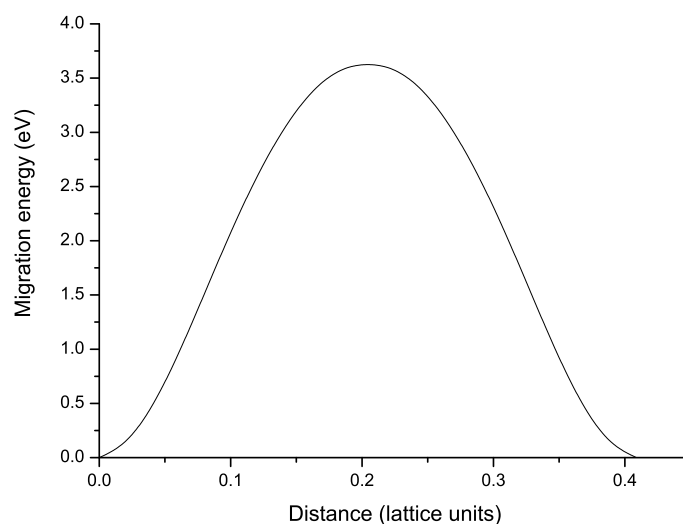


Figure 5.30: Migration energy for O^{2-} ion moving on O sublattice via vacancy mechanism 3.

5.3 Interstitial Migration

5.3.1 Magnesium Interstitial

In section 4.2.1 it was established that the intrinsic interstitial defects in MgAl_2O_4 spinel have a split structure in which two ions occupy a single lattice site. In the case of the magnesium interstitial two magnesium ions aligned in the $[110]$ direction share a single magnesium site. The ion positions before and after the migration process are shown by figure 5.31. It is clear that this is an interstitialcy mechanism as the migrating ion swaps places in the split, i.e. it initially is to the right of its shared lattice site in figure 5.31 but after migrating it is to the left of its lattice site. If the split interstitial is initially about the site at $(\frac{3}{4}, \frac{1}{4}, \frac{3}{4})$ and finally about the site at $(1, 0, 1)$ then the initial and final positions are, respectively, $(0.853, 0.139, 0.820)$ and $(0.889, 0.103, 0.922)$.

Figure 5.34 shows a very shallow local minimum at the interstitial site halfway between the two magnesium sites, however, it is only 0.01 eV lower in energy than at the twin saddle points which result in a barrier of 0.49 eV to migration via this mechanism. The energy profiles parallel and perpendicular to this migration path are shown in figures 5.32 and 5.33. The migration pathway is not straight as the Mg^{2+} ions move in such a way as to preserve the split structure whenever possible. The migrating ion nevertheless passes through the octahedral interstice halfway between the two magnesium sites, the point at which the ion forming a split with the migrating defect flips from the one

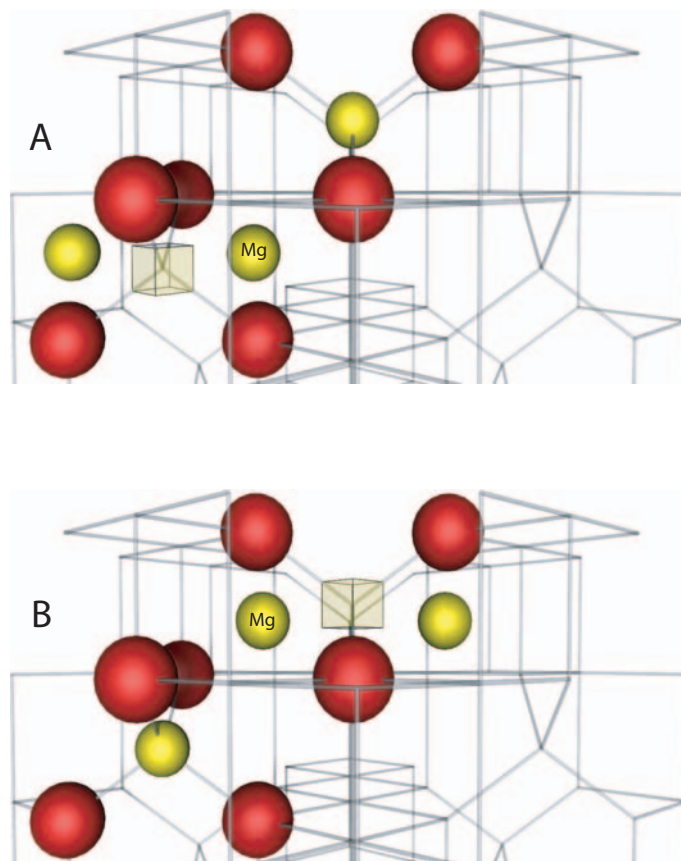


Figure 5.31: Schematic diagram showing ion positions before, A, and after, B, magnesium interstitialcy migration. Oxygen ions are red spheres, magnesium ions yellow spheres, and magnesium vacancies yellow cubes.

at the initial site to that at the final site.

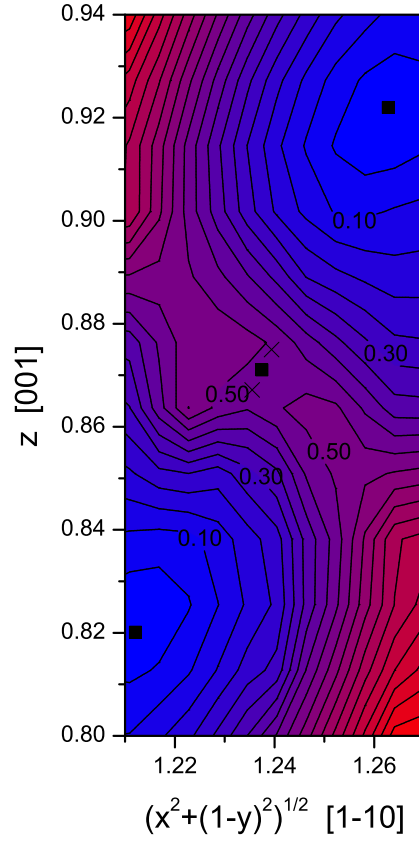


Figure 5.32: Energy contour plot for Mg^{2+} migration via a magnesium interstitialcy mechanism, parallel to the migration pathway.

5.3.2 Aluminium Interstitial

The aluminium interstitial structure described in section 4.2.1 is only metastable, a combination of $\text{Mg}_i^{\cdot\cdot} + \text{Al}_{\text{Mg}}$ is lower in energy by 2.2eV, if the defects are isolated. In fact, even when they are first neighbours the combination of Al_{Mg} and $\text{Mg}_i^{\cdot\cdot}$ is favoured. Consequently, given sufficient impetus aluminium in-

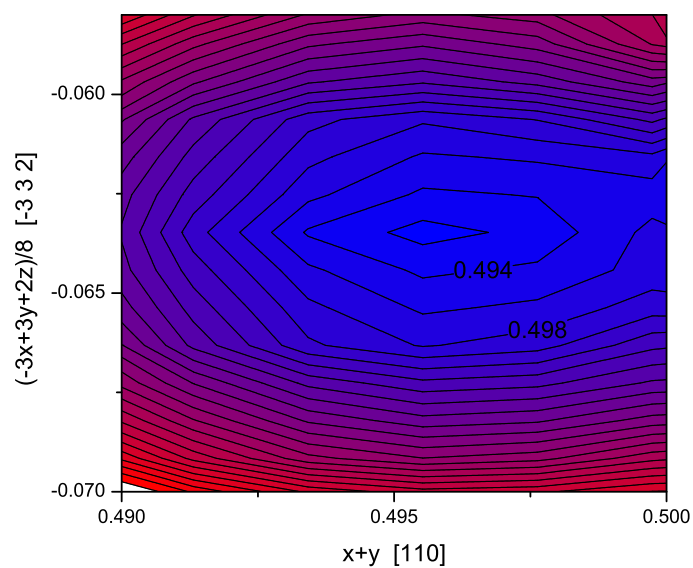


Figure 5.33: Energy contour plot for Mg^{2+} migration via a magnesium interstitialcy mechanism, perpendicular to the migration pathway.

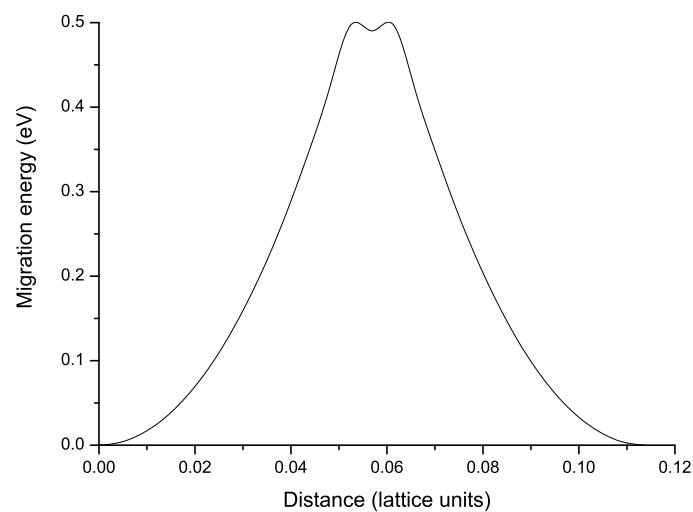


Figure 5.34: Energy profile along migration pathway for magnesium interstitial hop.

terstitial defects will collapse to a Al_{Mg} antisite, with the Mg^{2+} re-orienting to form a split Mg_i^{\cdot} with a neighbouring Mg^{2+} ion. As these defects are both positively charged it is expected that the additional Mg^{2+} ion will continue to migrate away.

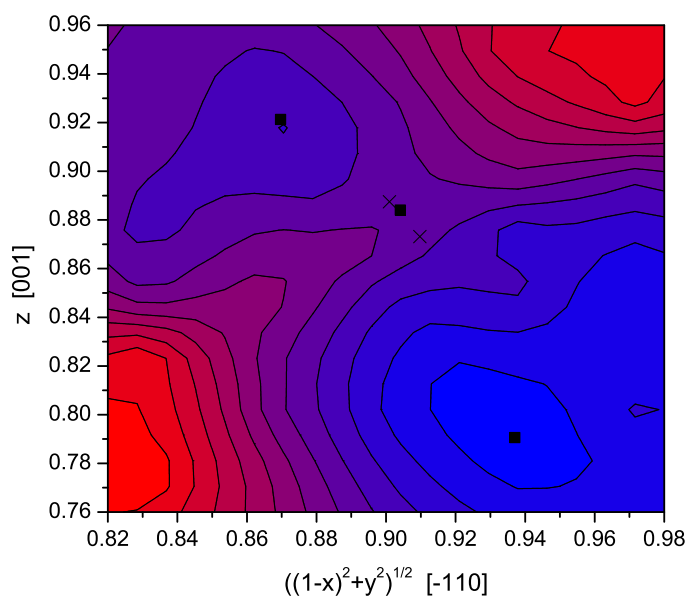


Figure 5.35: Energy contour plot for migration of Mg^{2+} between split aluminium and magnesium interstitial defects, parallel to the migration pathway.

Figures 5.35-5.37 contain the results of calculations on the aluminium interstitial system. The energy landscape is more complex than that seen for the magnesium interstitial, the migrating ion does not pass through the octahedral interstice, instead passing over one of two symmetric saddle points displaced either side of it in $[110]$ directions. Taking the initial aluminium interstitial to be sited around $(\frac{1}{2}, \frac{1}{2}, 1)$ and the final magnesium interstitial to be centered on $(\frac{1}{4}, \frac{3}{4}, \frac{3}{4})$, the higher saddle point, 0.54 eV, is at $(0.367,$

0.644, 0.887), the lower one, 0.52 eV, at (0.361, 0.648, 0.873) with the local minimum, 0.47 eV, in between at (0.364, 0.647, 0.881).

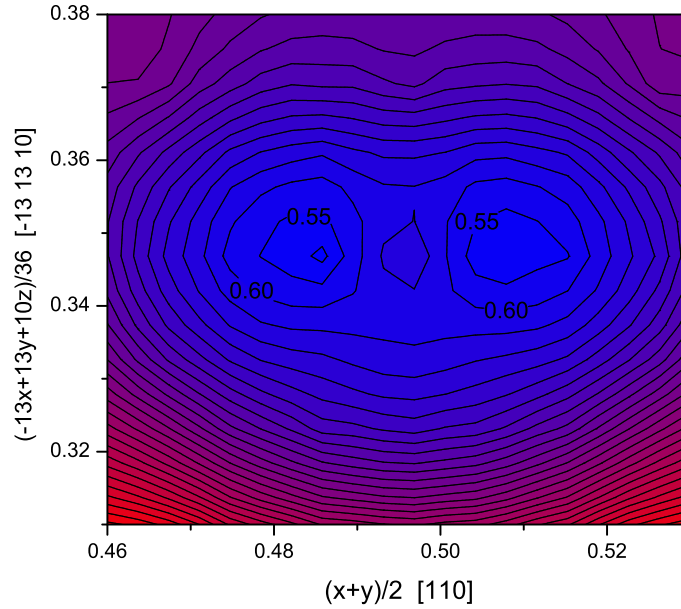


Figure 5.36: Energy contour plot for migration of Mg^{2+} between split aluminium and magnesium interstitial defects, perpendicular to the migration pathway.

5.3.3 Oxygen Interstitial

The split oxygen interstitial structure aligns itself along the same direction as the arrow representing mechanism 1 in figure 5.21, though neighbouring split pairs differ in [001] by approximately 0.08 lattice units. Figure 5.38 shows an equivalent plane to that in figure 5.21 with the two split interstitials in place. Similarly to the magnesium interstitial case the split structure of the interstitial defect means that this is an interstitialcy mechanism with only a

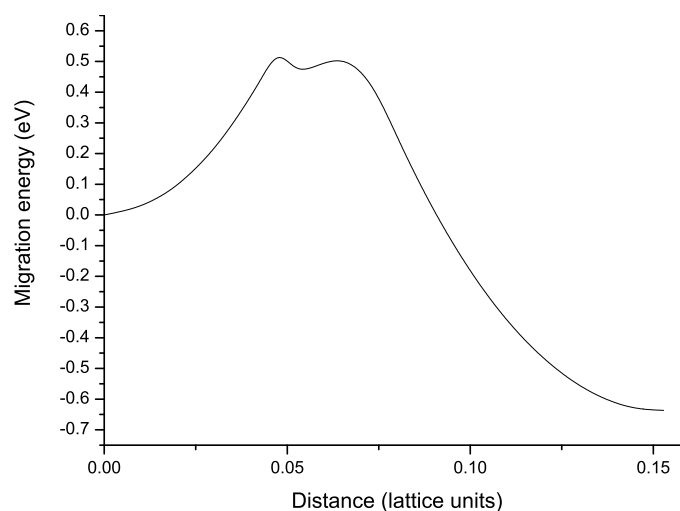


Figure 5.37: Energy profile along migration pathway for Mg^{2+} ion hopping between aluminium and magnesium interstitial defects.

small displacement between the start and end points.

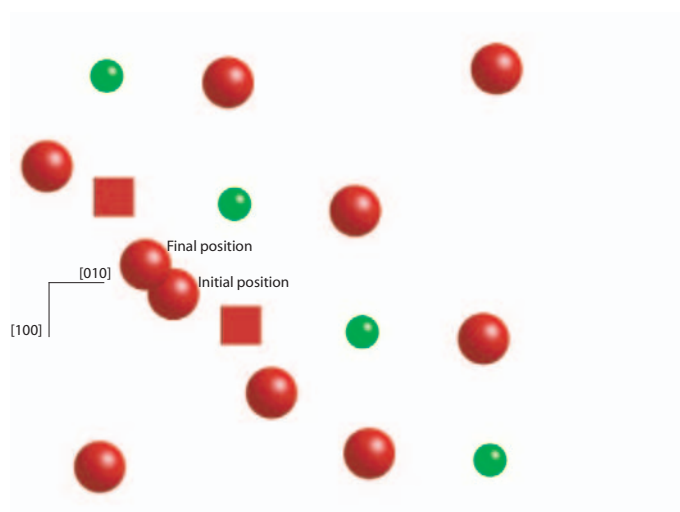


Figure 5.38: Cross section through a single unit cell of spinel showing the relative locations of ions forming two neighbouring split oxygen interstitials.

Figures 5.39 and 5.40 show that the interstitialcy migration pathway lies in

the plane perpendicular to that shown in figure 5.38 and the path, 5.41, is a straight line, in the $[\bar{3}\bar{3}\bar{4}]$ direction, with the saddle point halfway between the start and end points. The barrier is 0.28 eV, significantly lower than for magnesium, making the O_i'' the most mobile, intrinsic defect in MgAl_2O_4 .

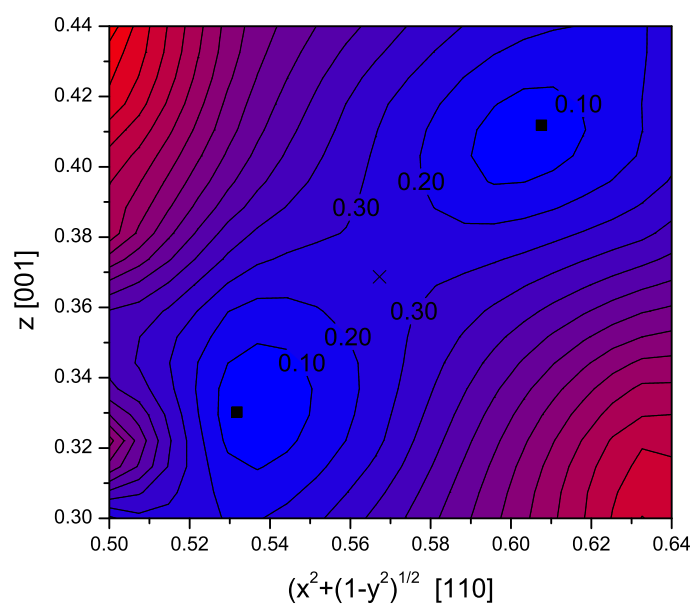


Figure 5.39: Energy contour plot for O^{2-} migration via an oxygen interstitialcy mechanism, parallel to the migration pathway.

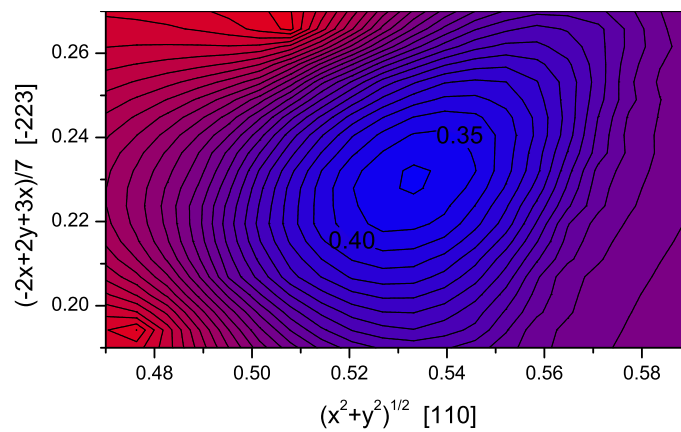


Figure 5.40: Energy contour plot for O^{2-} migration via an oxygen interstitialcy mechanism, perpendicular to the migration pathway.

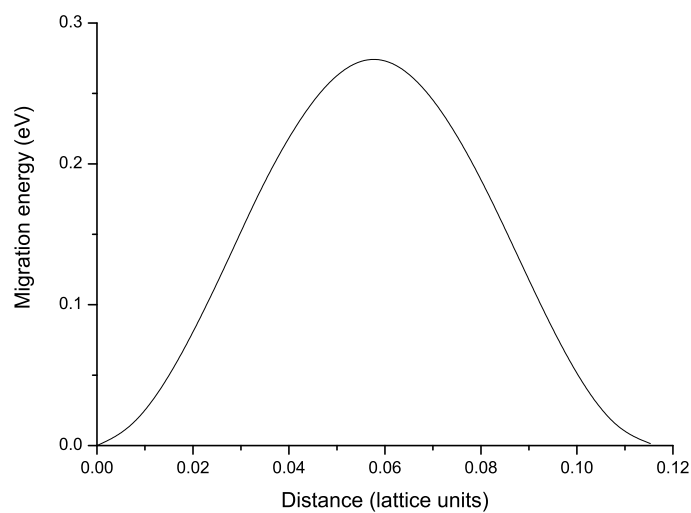


Figure 5.41: Energy profile along migration pathway for an oxygen interstitial hop.

5.4 Summary

Activation energies for migration of all the intrinsic defects discussed in this chapter are listed in table 5.1. The O_i'' has the lowest migration activation energy though both the Mg_i^\cdot and V_{Mg}'' have similarly small barriers. Of the cation defects magnesium is considerably more mobile in spite of its larger ionic radii in both tetrahedral and octahedral coordination (table 5.2), perhaps as a consequence of carrying a smaller ionic charge. The results for the aluminium diffusion are probably the most significant as they reveal that Al^{3+} will be transported on the magnesium sublattice, due to the presence of antisite defects.

The energy barriers for a cation vacancy to switch sublattices is large, which helps to explain the stability of antisite defects generated during simulated collision cascades [108, 144], assuming, of course, that antisite defects are created/destroyed via their interaction with vacancies.

Comparable experimental results are limited, though some experimental energies for self-diffusion exist. The diffusion energy contains both the defect formation energy and the activation energy for migration and as such is difficult to compare with the results presented here because, as was shown in chapter 4, the most favourable configurations for vacancy and interstitial defects in spinel involves the formation of clusters with charge compensating antisite defects. An experimental value for the oxygen self-diffusion of 4.55 ± 0.69 eV [138] is available. If it is assumed that the O_i'' is isolated from

any antisite defects in the lattice, then the value for comparison is $(6.25 + 0.28) = 6.53$ eV. If the O_i'' is allowed to form neutral clusters with nearby antisite defects then the predicted energy is reduced to $(3.14 + 0.77 + 0.28) = 4.19$ eV, much closer to the experimental value. This assumes, however, that the activation energy will not vary with the changed defect configuration of the migrating species. For magnesium (specifically the vacancy in this case) a value of 3.74eV [137], derived from diffusion data can be used for comparison. Again summing the defect formation energy and the migration energy, the value for comparison is $(5.32 + 0.55) = 5.87$ eV. As with the oxygen diffusion data the experimentally derived value is considerable lower than that calculated (assuming isolated defects). If, instead of the isolated defect formation energy, the energy to form the V_{Mg}'' as part of Schottky reaction producing trimer clusters is substituted, the calculated value becomes $(3.50 + 0.77 + 0.55) = 4.82$ eV. In contrast to the oxygen case the calculated activation energy for diffusion is still a little higher than the experimental value. It is not surprising that the absolute defect energies calculated in this way do not provide an exact comparison with experiment, however it might be expected that relative energies would allow for a consistent comparison with experiment. That this is not seen in this case is perhaps a consequence of the relatively large binding energy of $[\{\text{O}_i'' : 2\text{Al}_{\text{Mg}}'\}^\times]$ and $[\{\text{V}_{\text{O}}'' : 2\text{Mg}'_{\text{Al}}\}^\times]$ clusters. While the large binding energy of these clusters serve to reduce the predicted defect formation energy more than the comparable clusters for magnesium vacancies and interstitials it might be expected that this tighter binding would also increase the migration energy more than the more loosely

bound $[\{Mg_i:2Mg'_{Al}\}^\times]$ and $[\{V'''_{Al}:2Al'_{Mg}\}']$ do in the case of magnesium.

Table 5.1: Migration energies in MgAl_2O_4 spinel.

Migrating ion	Initial sublattice	Final sublattice	Mediating defect	Barrier (eV)
Mg^{2+}	Mg	Mg	V_{Mg}''	0.55
Al^{3+}	Mg	Mg	V_{Mg}''	1.15
Al^{3+}	Al	Al	V_{Al}'''	1.94
Mg^{2+}	Al	Al	V_{Al}'''	0.85
Al^{3+}	Al	Mg	$V_{\text{Mg}}'' \rightarrow V_{\text{Al}}'''$	2.66
Mg^{2+}	Mg	Al	$V_{\text{Al}}''' \rightarrow V_{\text{Mg}}''$	3.32
O^{2-}	O	O	$V_{\text{O}}^{\bullet\bullet}$	1.68
Mg^{2+}	Interstitial	Interstitial	$\text{Mg}_i^{\bullet\bullet}$	0.49
Mg^{2+}	Interstitial	Interstitial	$\text{Al}_i^{\bullet\bullet} \rightarrow \text{Mg}_i^{\bullet\bullet}$	0.54
O^{2-}	Interstitial	Interstitial	$\text{O}_i^{\bullet\bullet}$	0.28

Table 5.2: Ionic radii of cations in MgAl_2O_4 spinel [143].

Ion	Coordination	Radii (\AA)
Mg^{2+}	IV	0.57
	VI	0.72
Al^{3+}	IV	0.39
	VI	0.54